INTERNATIONAL JOURNAL OF CLIMATOLOGY
Int. J. Climatol. (2010)
Published online in Wiley Online Library
(wileyonlinelibrary.com) DOI: 10.1002/joc.2243

RMetS
Royal Meteorological Society

Sky view factor analysis of street canyons and its implications for daytime intra-urban air temperature differentials in high-rise, high-density urban areas of Hong Kong: a GIS-based simulation approach

Liang Chen,* Edward Ng, Xipo An, Chao Ren, Max Lee, Una Wang and Zhengjun He
School of Architecture, The Chinese University of Hong Kong, Shatin, N. T., Hong Kong S. A. R., P. R. China

ABSTRACT: Hong Kong is a high-density sub-tropical city with 7 million people living in an urban area of just over 260 km^2. Tall and closely packed buildings are the common urban morphology. How the urban geometry influences the microclimate in summer daytime is a primary planning concern. The sky view factor (SVF) has been commonly used to indicate the impact of urban geometry on air temperature differences in cities. However, only limited discussions in this aspect have been addressed for daytime course in high-rise and high-density urban environment such as Hong Kong. This paper firstly provides a comprehensive review of SVF analysis in urban climatology studies and then presents a simulation approach to investigate the role of SVF in determining summer daytime intra-urban air temperature differences in urban Hong Kong. An ArcGIS-embedded computer program is developed for calculating continuous SVF values for an entire urban environment and an SVF map is generated. The result is evaluated against meteorological data observed in field measurements. The regression analysis shows that the spatial average of SVF values has a close negative relationship with daytime intra-urban temperature differences. The study indicates that SVF is a significant factor for understanding the microthermal climate in Hong Kong's street canyons. The paper further raises discussions on the application of SVF analysis to urban planning. The study demonstrates that the SVF analysis is a useful and effective tool for planners and urban climatologists conducting studies on high-rise and high-density sub-tropical cities. The understanding can provide support for the development of planning standards and good practice. Copyright © 2010 Royal Meteorological Society

KEY WORDS sky view factor (SVF); urban climate; intra-urban air temperature difference; Geographic Information System (GIS)

Received 10 April 2010; Revised 4 September 2010; Accepted 25 September 2010

1. Introduction

Hong Kong is a high-density city located on the coastline of South East China (22°15′N, 114°10′E) with an average altitude of 8 m. It has a sub-tropical climate with hot, humid and long summer months lasting from May to September. The summer average temperature is around 28.5 °C (Hong Kong Observatory, 2010). This has already some impact on urban thermal comfort. Being one of the most densely populated cities in the world, Hong Kong has its 7 000 000 population living in around 260 km^2 of developed land. The urban density of some metro areas can be as high as 50 000 inhabitants/km^2 (Planning Department, The Government of Hong Kong S.A.R., 2008; Census and Statistics Department, The Government of Hong Kong S. A. R., 2009). Tall buildings of some 40–60 storeys lining narrow streets of 15–25 m have been the norm (Figure 1). This has created a kind of canyon that has never been witnessed in any other part of the world (Figure 2). How the buildings impact the local microclimate and, therefore, human thermal comfort in summer daytime has been a primary planning concern.

Urban geometry has a complex influence on the microclimate of an urban environment. The most important effect is that building bulks obstruct open sky and delay the cooling of the surface during clear and calm nights and result in the urban heat island (UHI) phenomenon (Oke, 1981). A commonly used indicator to describe the urban geometry is the sky view factor (SVF). As the name implies, the SVF, often denoted by ψ_{sky}, indicates the ratio of the radiation received (or emitted) by a planar surface from the sky to the radiation emitted (or received) from the entire hemispheric radiating environment (Watson and Johnson, 1987). Owing to its important role in radiation balance schemes, SVF has been widely used by climatologists to investigate the relationships between urban geometry and nocturnal UHI intensity (Lindqvist, 1970; Oke, 1981; Bärring *et al*., 1985; Yamashita *et al*., 1986; Eliasson, 1990–1991; Upmanis and Chen, 1999; Svensson, 2004; Gal *et al*., 2009; Unger, 2009). Unger (2004) has provided a comprehensive review of research work in this domain.

* Correspondence to: Liang Chen, Room 701, Wong Foo Yuen Building, School of Architecture, The Chinese University of Hong Kong, Shatin, N. T., Hong Kong S. A. R., P. R. China.
E-mail: chenliang@cuhk.edu.hk

Figure 1. Hong Kong's high-rise and high-density built-up area. (Source: http://www.globalphotos.org).

Figure 2. A sky view in Hong Kong's typical street canyon. (Source: authors).

In contrast with the commonly observed positive nocturnal UHI effect, where the urban built-up area is normally warmer than rural non-built-up area at night, the investigations into daytime UHI present a scattered picture. While positive daytime UHI has been observed in various climates such as cities in Greece, USA, Puerto Rico and China (Stathopoulou and Cartalis, 2007; Hart and Sailor, 2009; Murphy *et al*., 2010; Yang *et al*., 2010), negative daytime UHI, often referred to as urban cool island (UCI), has also been observed in UHI studies across the world (Morris and Simmonds, 2000; Alonso *et al*., 2003; Chow and Roth, 2006; Mayor of London, 2006). These contradictory results reflect the complexity of the cause of daytime UHI; on the other hand, they are also due to the diversity of the surveyed environment, such as different land use and the presence of tree canopy.

For the high-rise and high-density urban environment of Hong Kong, negative daytime UHI has been revealed mainly by comparing temperature measurements at Hong Kong Observatory stations located in urban and rural areas. For example, Chan and Ng (1991) found that the average summer maximum temperature recorded at urban street canyons was over 0.6 °C lower than that of satellite towns and rural areas; Wu *et al*. (2008) reported that between 10 am and 5 pm, the negative UHI, calculated by the annual average of hourly temperature, was up to 1 °C; similar results were also found in Leung and Lee (2010). Given that Hong Kong is a heavily urbanized city, what is more interesting to know is how the air temperature varies in the intra-urban area. As pointed out by Eliasson (1996): "A good knowledge of the influence of street geometry on temperature over very short distances, within cities, would be of great value, not least for urban planning." However, relevant discussions are still sparse for Hong Kong. Limited studies have observed that the daytime intra-urban temperature difference between built-up and non-built-up areas could be either positive or negative (Giridharan *et al*., 2004; Fung *et al*.; 2009). One special interest with this aspect is to investigate the air temperature variations with regard to Hong Kong's unique urban geometry. However, related literature only addressed limited discussions in an SVF framework, though it has been shown to describe the urban geometry effectively. There are two reasons for this issue:

1. Estimation of SVF for an entire urban environment in the real world is never an easy task. Conventional methods often employed photographic techniques (e.g. fish-eye photo) where only scattered spots are investigated. Although more effective methods such as software methods have been developed, they are not widely accessible. Owing to the limited SVF data, more comprehensive SVF analysis, which is expected to provide more understanding of air temperature variation pattern, is not possible.
2. Spatial correlation of SVF and air temperature differences is not evident. Earlier studies in Hong Kong are not placed in a geographically defined framework, so spatial analyses such as spatial average and sampling are quite limited.

The objective of this study is to analyse the effect of urban geometry, quantified by SVF, on summer daytime intra-urban air temperature differences in Hong Kong's street canyons. Summer is selected because it is Hong Kong's most crucial season in terms of thermal load and thermal comfort. A GIS-based simulation approach is taken where an ArcGIS-embedded computer program is developed for calculating continuous SVF values for an entire urban environment. Three-dimensional (3-D) GIS-based dataset of Hong Kong is used and an SVF map is generated. Field measurements are carried out to survey the spatial variation of air temperature. The relationship between SVF and air temperature differences is investigated by means of regression analysis. The spatial average of SVF is used in the analysis. The derived relationship is used to give recommendations in planning applications.

2. Literature review

2.1. Determination of SVF

SVF in an urban environment is commonly determined by four types of methods: analytical methods, photographical methods, Global Positioning System (GPS) methods or software methods, developed in an approximately chronological order. This section reviews the four methods.

2.1.1. Analytical methods

Analytical methods are also referred to as geometrical methods. They base the estimation of SVF on the geometrical characteristics and radiation exchange model of the urban canyons. For a general case, Johnson and Watson (1984) calculated SVF by analysing the fraction of the radiation flux leaving a studied surface element that reaches the visible sky, and gave

$$\psi_{\text{sky}} = \frac{1}{\pi R^2} \int_{S_v} \cos \Phi dS \tag{1}$$

where S_v is the section representing the visible sky, Φ is the angle from S_v to the zenith, and R is the radius of the hemispheric radiating environment.

Oke (1981) considered the wall view factor and simplified the model by defining an infinitely long urban canyon with height H and width W ($W = 2\ D$). With this simplification, SVF at the centre point of the two walls was defined by

$$\psi_{\text{sky}} = \cos \beta \tag{2}$$

where β is the elevation angle of the wall and $\beta = \tan^{-1}(H/D)$. This suggests that SVF can be approximated by height/width ratio (H/W) for regular-shaped street canyons. Oke (1987) also derived SVF for other simplified models (in the same notation): For a completely enclosed circular basin,

$$\psi_{\text{sky}} = \cos^2 \beta \tag{3}$$

For an infinitely long wall or slope,

$$\psi_{\text{sky}} = \frac{(1 + \cos \beta)}{2} \tag{4}$$

For an infinitely long valley,

$$\psi_{\text{sky}} = \cos \beta \tag{5}$$

In reality, buildings in urban canyons are always asymmetric in shape and of finite dimension, which requires refinement of the equation. Johnson and Watson (1984) used azimuth angles (γ_1, γ_2 from the studied surface element ΔA to the two ends of the wall) and elevation angle (β) of surrounding buildings and calculated wall view factor ψ_w for ΔA as

$$\psi_w = \frac{1}{2\pi}\{(\gamma_1 - \gamma_2) + \cos \beta[\tan^{-1}(\cos \beta \tan \gamma_1) - \tan^{-1}(\cos \beta \tan \gamma_2)]\} \tag{6}$$

Then ψ_{sky} was given by

$$\psi_{\text{sky}} = 1 - \sum_{i=1}^{n} \psi_w(i) \tag{7}$$

where n is the number of buildings surrounding ΔA.

The analytical methods give a theoretical framework for determining SVF for a particular point in different urban structures. They are suitable for simple and well-represented structures and can be used for algorithm testing and parametric analysis.

2.1.2. Photographic methods

The photographic methods use a fish-eye lens to take on-site photographs that project the hemispheric environment onto a circular plane. The photographs are then processed (converting colour to grey image, altering brightness and contrast, etc.) to define the skyline. The relation between obstructed and unobstructed parts of the sky is then calculated by appropriate transformations. Some methods employing video imagery techniques (Bärring *et al.*, 1985; Steyn *et al.*, 1986) also generally fall into this category, as they also base their work on fish-eye lens photograph processing. Anderson (1964) was probably the first one who considered the view factor issue through a photographic approach when she used photographic computation to estimate sunlight distribution in her forest canopy studies, but it is only since the 1980s that photographic methods have received enough attention in determining SVF in urban climatology research. Steyn's (1980) equiangular projection is the most commonly used method. He divided the projected image into a number of concentric annuli of equal width, and then by summing up all the annular sections representing the sky, he estimated SVF by

$$\psi_{\text{sky}} = \frac{1}{2n} \sum_{i=1}^{n} \sin\left[\frac{\pi(i - 1/2)}{2n}\right] \cos\left[\frac{\pi(i - 1/2)}{2n}\right] \alpha_i \tag{8}$$

where n is the total number of annuli, i is the annulus index and α_i is the angular width of sky in the ith annulus.

Johnson and Watson (1984) later suggested a modified version of Steyn's method:

$$\psi_{\text{sky}} = \frac{1}{2\pi} \sin \frac{\pi}{2n} \sum_{i=1}^{n} \sin\left[\frac{\pi(2i - 1)}{2n}\right] \alpha_i \tag{9}$$

demonstrating that Steyn had approximated $\sin[\pi/(2n)]$ by $\pi/(2n)$ when n is large enough (37 in his case).

On the basis of their theoretical framework, the photographic technique was further developed by extending the projection to unequiangular cases (Blennow, 1995), and by employing more powerful hardware and software (Chapman *et al*., 2001; Grimmond *et al*., 2001; Gal *et al*., 2007; Rzepa, 2009).

The photographic technique is particularly suitable for determining SVF in real cases in that it can deal with buildings of various sizes and irregular shapes. Vegetation information is also present in the photographs so that precise SVF can be obtained, whereas other methods may result in errors under this situation (Grimmond *et al*., 2001; Gal *et al*., 2007). However, this method requires image generation and processing, and therefore is often time-consuming. Also, surveying opportunities for this method are limited, as a homogeneous cloudy sky is normally required; direct sunlight or different cloud type will cause problems in image processing (Chapman and Thornes, 2004). Furthermore, spatial information of the studied points is not present or needs to be managed in separate datasets. These limitations make the photographic methods unsuitable for large area analysis.

2.1.3. GPS methods

In contrast to the above-mentioned methods, which are based on direct calculation of SVF, the GPS method (Chapman *et al*., 2002) was developed with the aim of measuring SVF in real time using proxy data. A GPS receiver was used to acquire raw data of satellite visibility. The number of visible satellites, dilution of precision and strength of satellite signal were used in multiple regression analysis to derive a regression equation for the prediction of SVF. The method was shown to generate good results in urban environments but had a reduced explanation power in suburban and rural environments, which was consistent with the expectation that the variation in tree cover would produce noise in signal processing. The prototypical method was further developed by Chapman and Thornes (2004) to produce instant SVF calculation. The GPS component was integrated with a fish-eye lens photo capturing and processing module on a mobile platform to give simultaneous calculation and approximation of SVF in real time. An artificial neural network was trained to predict SVF based on three parameters: the number of tracked satellites, the number of visible satellites and the sum of signal-to-noise ratios. The application could explain over 69% of SVF variations in urban areas, with a processing rate of 1 s.

Several features of the GPS methods make them more appealing than the traditional methods: (1) they are rapid and relatively inexpensive, (2) the survey is not dependent on atmospheric condition as opposed to photographic methods and (3) they can be easily linked with the geographic information system (GIS) platform. However, the methods still have limitations that restrict them to only limited applications. Firstly, by nature the methods are not exact, which indicates that they are not suitable when accuracy is essential; secondly, the prediction equation depends on the GPS equipment used, so it is impossible to derive a universal equation and thirdly, the performance of the method is good only for urban areas.

2.1.4. Software methods

The development of land survey and digital mapping techniques, together with the rapidly increasing computer power, opens up new possibilities to describe the urban geometry from a 'virtual' aspect. Software methods employ building database, commonly GIS-based 3-D models, and reconstruct the urban environment in the computer's memory. Computer programs are developed to simulate SVF in the reconstructed world. Depending on the types of database used, there are two main approaches of software methods: vector method and raster method.

The vector database simplifies buildings by flat-roofed blocks represented by polygons. The hemispheric radiating environment is divided equally into slices by a rotation angle. Then, along a particular rotation angle, the method searches for a single building with the largest elevation angle along that direction. The sky segment obstructed by this building is considered as a slice of the basin as examined in Oke's (1987) discussion (refer to Equation (3)). Then SVF can be calculated by summing up the view factors of all the basin slices for all directions (Gal *et al*., 2009). The accuracy of this method depends on the rotation angle and the searching radius: smaller rotation angle and larger radius result in more accurate SVF estimation.

The raster-based method is another commonly used way to determine SVF. A digital elevation model (DEM) database is often employed where surface topography and terrain information are stored in raster format. Ratti and Richens (1999) have developed a 'shadow casting' algorithm that calculates building shadow patterns based on high-resolution DEM. This algorithm is further modified to calculate SVF and has been validated by Lindberg (2005) to generate satisfactory results. The raster-based method has been proved to be 'significantly faster' than the vector-based method (Gal *et al*., 2009). The accuracy of the method depends on the resolution of the raster database: higher resolution results in a more accurate result.

The software methods depend to a great extent on the availability of building database. On the other hand, they offer rapid ways to calculate continuous SVF for large areas based on which comprehensive analysis could be carried out. They are becoming increasingly widely recognized in recent studies.

2.2. Analysis of SVF's effect on daytime air temperature difference

Despite the substantial literature of studies on the effect of SVF on nocturnal UHI (refer to Section 1), only limited discussions have been raised for the daytime case. In the comprehensive review by Unger (2004), only two reviewed studies dealt with daytime temperature differences (Santos *et al*., 2003; Vieira and Vasconcelos,

2003). As opposed to the commonly agreed on SVF–ΔT relationship in nocturnal cases, which is that smaller SVF normally results in higher temperature at night, neither study found a clear correlation between SVF and temperature difference. Atkinson (2003) used a numerical model to simulate the UHI intensity in an idealized urban configuration. Through control experiments, he found that the absence of SVF weakened the mid-morning UHI by about 0.3 °C. However, the SVF parameter covered only two cases, being 1 as rural value and 0.4 as urban value, so the study provided little implication for intra-urban cases. Steemers *et al*. (2004) alternatively correlated SVF with *temperature swing*, which is the degree of adhesion to synoptic conditions. On the basis of temperature measurement data collected in Cambridge on a spring morning, they found that larger SVF resulted in higher temperature swing, indicating that less densely built-up areas would follow the ambient environment more closely. The relation was used to explain the daytime UCI in deep courtyards. What is interesting is the derived logarithmic relationship [$T_{swing} = \ln(1 + SVF/0.02)/0.35$] when compared with conventional linear relationships. As the surveyed area has an average SVF of 0.7, whether the relationship could be applied to the dense case of Hong Kong is questionable. Bourbia and Boucheriba (2010) studied the impact of street design on the microclimate in the very dense centre of a North African city with a semi-arid climate. The street geometry was expressed by SVF estimated from fish-eye lens photographs and H/W ratio. A total number of seven stations were examined, with SVF ranging from 0.076 to 0.58. Temperature was measured in the summertime of July representing the hottest period. By comparing the diurnal average temperature and SVF, it was found that an increase in SVF would lead to a higher temperature. Although the authors stated that SVF 'had a strong influence on air temperature between the hours of 12 am to 6 pm with an $R^2 = 0.46$', no correlation equation was given and it is not clear how many stations were used in the regression analysis.

In the Hong Kong case, discussions are even more limited in a ΔT–SVF scheme. Giridharan *et al*. (2004) have pilot-investigated the impact of SVF, as one component of a group of influential factors, on daytime UHI in Hong Kong's residential developments. The investigation was only a micro-scale study carried out in three large housing estates, and only three SVF values were calculated based on analytical methods, being 0.373, 0.473 and 0.470. Multivariable analysis showed that the regression coefficient of SVF for daytime UHI (in the order of 1.5 °C) could be either positive or negative. The authors attributed this to different building structures, but without further elucidating the interrelationship. In a later study, Giridharan *et al*. (2007) further extended the investigation to a still small sample size of 17 residential developments. The SVFs for each location were derived from on-site fish-eye lens photographs, with numerical values ranging from 0.11 to 0.59. The limited study revealed that, in peak summer clear sky days, all 12 variables, including SVF, surface albedo, wind speed, etc., could collaboratively explain daytime UHI changes 'consistently', with a positive coefficient sign of SVF. Despite the high determination coefficient (0.7), it is difficult, both in technical and planning terms, to derive a relationship between SVF and temperature variation patterns from the study because of the interweaving of SVF with other factors. The limited studies, therefore, have little useful application.

So far most of the studies have employed photographic methods to measure SVF for selected sites. A new approach (Unger, 2004), which compares the areal average of both geometry and temperature variations, is confirmed to be useful in clarifying the ΔT–SVF relationship (Gal *et al*., 2009). An investigation into this framework, with both extensive temperature measurement and comprehensive SVF analysis, is yet to be conducted for Hong Kong.

3. Development of a rapid software method to compute continuous SVF values

In this study, a rapid software method is developed to compute continuous SVF values for an entire urban environment using a 3-D GIS-based database. A computer program is developed in VBA programming language and embedded as a macro in the ArcGIS system. SVF maps for entire areas can be generated. The GIS-based feature of the present method makes it suitable for collaborating with spatially related dataset such as measurement data over a large area.

3.1. Algorithm and methodology

A hybrid algorithm is developed which shares the same geometrical arrangements and theoretical basis with the vector method proposed by Gal *et al*. (2009), but uses high-resolution raster as input data. A 3-D building database (with building height information) is merged with the topography database to create a DEM layer representing the height of the urban surface. The building database is also used to create a Mask layer representing built-up and non-built-up areas. The Mask layer can easily control whether building top is included in the SVF calculation. In case only ground level SVF is needed, the algorithm scans the extent of the Mask layer and calculates SVF for each pixel of non-built-up area. The result is stored with geographic information in a raster database. An illustration of the algorithm is shown in Figure 3.

For a point Po, as discussed in Section 2.1.4, the algorithm divides the hemispheric radiating environment with radius R into equal slices by a rotation angle α and searches for a pixel Pi with the largest elevation angle β along a particular direction. β is determined by $\tan^{-1}(h(\mathrm{Pi})/r)$, where h(Pi) is the height difference between Pi and Po, and r is the distance from Pi to Po. In case Pi is found, the surface S, which is a slice of an enclosed basin, is considered to be obstructed. According to Equation (3), the view factor of S is $\mathrm{VF(S)} = (1 - \cos^2\ \beta) \cdot (\alpha/360)$

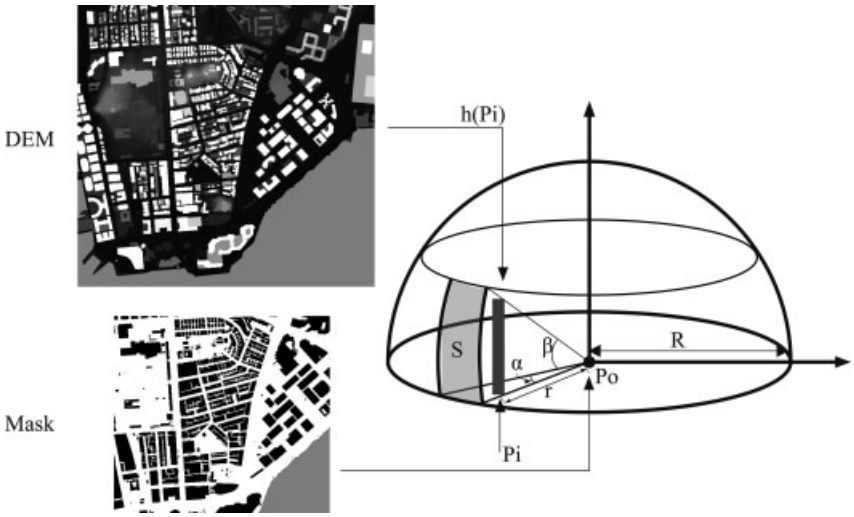

Figure 3. Illustration of the algorithm for calculating SVF. The Mask layer defines the pixels whose SVFs are to be calculated (Po) and the DEM layer stores height information of the urban surface (h(Pi)). α is the rotation angle and R is the searching radius. Pi is the pixel with the largest elevation angle β along a certain direction. Surface S is the segment of the sky obstructed by Pi.

$= \sin^2 \beta \cdot (\alpha/360)$, so the SVF of Po can be calculated by summing up the VF(S) for all the directions and subtracting the sum from unity.

3.2. Verification of the method

The software method is verified by comparing the simulated SVF with results from the analytical method and the fish-eye lens photographs. Two parametric models suggested by Oke (1987) are tested for comparison with the analytical method. The first one is an enclosed circular basin with a 20-m-high building and a 40-m diameter central space. The second model is a 2-km-long street canyon (representing an infinitely long case), with a 20-m-high building and a 40-m-wide street. The software method uses a rotation angle of 1° and a radius covering the whole scope of the model (50 m for the basin model and 1.1 km for the canyon model). The comparison between SVF results calculated by the analytical and software methods is shown in Table I. The result is generally satisfactory.

Fish-eye lens photographs are also used to verify the software method's applicability to real urban environment. Six photographs are taken in Hong Kong's densely built-up areas with little vegetation. The photographs are taken at 1.5 m above ground level, using a digital camera, Nikon FM601, with an 8-mm circular lens. The BMSky-view software (Gal *et al*., 2007; Rzepa, 2009) is used to process the images and calculate SVF. The results are compared with SVF simulated by the software method using 1° rotation angle and 500 m radius. As shown in Figure 4, the SVF values from the software method are constantly higher than those from the photographic method, but the differences are reasonably small (<0.05). Because of the absence of vegetation, the differences are much smaller than those found by Gal *et al.* (2007). The applicability of the software method in Hong Kong's urban environment is confirmed.

Table I. Comparison between SVF results calculated by analytical method (SVF(a)) and software method (SVF(s)) for two ideal cases: (1) an enclosed circular basin and (2) an infinitely long canyon.

	Basin case	Canyon case
SVF(a)	0.5000	0.7071
SVF(s)	0.5062	0.7218

3.3. Performance

Because of its hybrid feature, the algorithm's accuracy depends on three factors: the rotation angle α, the hemisphere's radius R and also the raster resolution. The resolution of the dataset is 2 m, and then the other two parameters need to be selected properly. Generally, a smaller rotation angle and a larger radius will result in more accurate SVF estimation; on the other hand, they will also lengthen the computing time. An example site of built-up area in Hong Kong with significantly diverse SVF ranging from 0 to 1 is used to test the method's performance with different parameter settings. In Section 3.2, it is found that 1° rotation angle and 500 m radius lead to a satisfactory result, so SVF calculated with this setting is used as the standard value. When the rotation angle is changed to 2° with the same radius, no difference is found in the result; however when it is changed to 3°, a substantial difference up to 0.23 occurs. So a rotation angle of 2° is selected. For the radius, three radii are compared with the standard, being 100, 200 and 300 m. Table II gives a summary of the comparison. It is found that compared with a 500-m radius estimation, the maximum SVF difference in street canyons is very small for all cases, being 0.005, 0.003 and 0.001 for 100, 200 and 300 m radius respectively. However, the maximum SVF difference in the domain can be up to 0.174 for 100 m radius and the difference is significantly reduced

SVF: fish-eye	0.420	0.282	0.410	0.210	0.237	0.204
SVF: simulated	0.442	0.288	0.420	0.258	0.275	0.239

Figure 4. Comparison of SVF calculated by fish-eye lens photos and the software method.

Table II. Comparison of the accuracy of three different radii (100, 200 and 300m).

	R = 100 m	R = 200 m	R = 300 m
Largest SVF difference in domain	0.174	0.059	0.031
Largest SVF difference in street canyons	0.005	0.003	0.001

SVF calculated with 500 m radius is used as standard value for comparison.

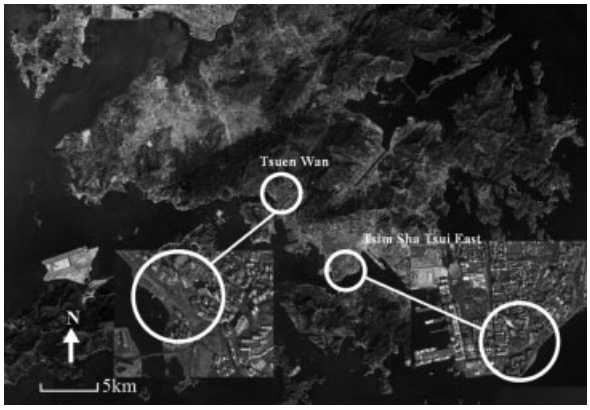

Figure 5. Google™ map of study sites: TST and TW.

with larger radius, being 0.059 for 200 m and 0.031 for 300 m radius. Balancing the accuracy and the computing time, a radius of 200 m appears to be appropriate, which was also the parameter selected by Unger (2009). So a radius of 200 m is used in practice.

Compared to the commonly used 'shadow casting' algorithm in raster-based software methods (Ratti and Richens, 1999; Lindberg, 2007, Gal *et al.*, 2009), the present method has an advantage in that it does not involve marginal error, i.e. once the radius is decided, the DEM layer can be prepared accordingly so every calculated pixel in the Mask layer has a correct value (refer to Figure 3). Optimizations are also made to accelerate the algorithm. On a daily used PC with 3 GHz CPU and 4 GB RAM, the method calculates continuous SVF for an entire terrain of size 2×2 km within 1 h, which is a huge improvement compared with the traditional photographic method.

4. Case study: daytime intra-urban air temperature variation analysis

In this study, two sites in Hong Kong's most densely built-up areas are selected for investigating the impact of SVF on summer daytime intra-urban air temperature differences: Tsim Sha Tsui East (TST) of size 1.8×1.8 km and Tsuen Wan (TW) of size 2×1.8 km. Both sites are coastal flat terrains of similar land use category (mostly commercial and residential development) with little vegetation (Figure 5). Differences in building height and density are commonly found in the domain. In the TST site, there are over 1400 buildings and the average building height is 42.5 m with a deviation of 27.0 m. Similar figures can be found in the TW site. An initial investigation is carried out in the TST site to study the relationship between SVF and temperature variations. The TW site is used to validate the applicability of the revealed relationship.

4.1. Temperature measurement in TST

Two field measurements were carried out in TST on calm summer afternoons to observe air temperature differences in street canyons: one on 19 September 2006 and another on 9 September 2008. Climatic conditions of the measurements are given in Table III. The 2006 measurement collected a larger dataset which is used in regression analysis, and the smaller dataset collected in 2008 measurement is used to verify and calibrate the derived relationship. Similar methodologies were used for both measurements. The following discussions are based on the descriptions of the 2006 measurement.

Twelve researchers were divided into six groups to conduct synchronized spot measurements along six pre-selected routes, generally starting from the seafront to the inner built-up area (Figure 6). The measurement spots were chosen to cover built-up areas of various densities and a total number of 48 points were selected. The time interval between two measurement spots was 10 min. Measuring equipments were held at 2 m above ground level, including a three-function sensor probe from TESTO 400 for the measurement of air temperature, relative humidity and wind speed, and TESTO 400 data logger for instant processing of measured data. The data logger was set to have a sampling time of 10 s and an averaging time of 3 min. All equipments were ISO certified and calibrated in the laboratory beforehand. During the measurement period, instantly updating climatic data from the Hong Kong Observatory website

Table III. Summary of climatic conditions of field measurement in TST, including air temperature (T), global solar radiation (Radiation), relative humidity (RH), wind speed (V) and duration of sunshine (Sunshine).

Date	Measurement period	T (°C)	Radiation (W/m^2)	RH (%)	V (m/s)	Sunshine (h)
19 September 2006	14 : 30–16 : 30	27.7–29.4	250–416	60–65	1.7–4	10
9 September 2008	14 : 30–15 : 30	31.6–32.5	630–800	≈60	2.5–4	10.6

The data were recorded by the Hong Kong Observatory at a station next to the study area.

Figure 6. Temperature measurement map for TST site.

(http://www.weather.gov.hk/) was also downloaded for reference. Detailed specifications of the measurements are given in Ng *et al*. (2008b).

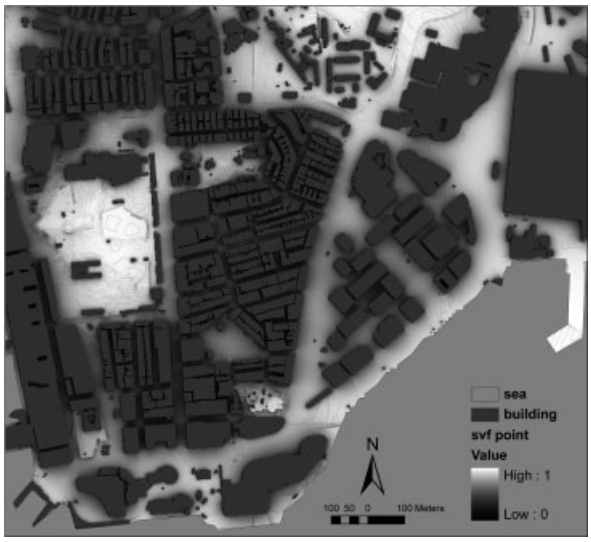

Figure 7. Ground-level continuous SVF map for TST site.

4.2. Data analysis and correlation

Measured data are time-corrected with the Hong Kong Observatory station assuming that temperature changes at the same pace within the pasture. The quantity of interest here is not the absolute temperature but the temperature difference (Streutker, 2003). The lowest temperature was recorded at a reference point located at an open space near the seafront, being 28.0 °C. Temperature differences for all measured points are calculated. Five points next to a high traffic road and two points close to the exits of a major metro station are deleted to eliminate traffic-induced turbulence. Finally, a total number of 41 points are examined. It is observed that temperature differences are commonly found in street canyons, with maximum value up to 4.9 °C.

A map of continuous SVF at the ground level for the entire area is generated using the developed method introduced in Section 3 (Figure 7). Then with the help of ArcGIS system, the temperature differences are coded into the continuous SVF map by manually drawing the examined points according to the measurement map. SVF values for each point are then extracted using the software built-in functions. Through regression analysis, a linear correlation of ΔT and point SVF value is derived, as shown in Table IV. The regression shows a general trend of SVF's negative impact on temperature differences, which indicates that smaller SVF generally leads to higher temperature difference, however, with relatively low determination coefficient ($R^2 \sim 0.18$).

Table IV. Summary of correlations of ΔT and SVF for five cases of SVF analysis: point value (point), 50 m radius neighbourhood average, 100 m average, 150 m average and 200 m average.

Case	Regression equation	R^2	α (%)	RMSE	Valid SVF range
Point	$\Delta T = -3.0369 \times \mathrm{SVF} + 4.051$	0.1765	5	1.135	$0.1 \leq \mathrm{SVF} \leq 0.75$
50 m	$\Delta T = -5.4793 \times \mathrm{SVF} + 5.0054$	0.485	5	0.8977	$0.15 \leq \mathrm{SVF} \leq 0.7$
100 m	$\Delta T = -6.6595 \times \mathrm{SVF} + 5.6061$	0.6503	5	0.7055	$0.2 \leq \mathrm{SVF} \leq 0.75$
150 m	$\Delta T = -7.5165 \times \mathrm{SVF} + 6.049$	0.6584	5	0.7311	$0.2 \leq \mathrm{SVF} \leq 0.75$
200 m	$\Delta T = -8.6344 \times \mathrm{SVF} + 6.6914$	0.5289	5	0.8586	$0.3 \leq \mathrm{SVF} \leq 0.7$

The correlations are summarized by regression equation, coefficient of determination (R^2), significance level (α), root mean square error (RMSE) and valid SVF range.

Unger (2004) has shown that the comparison of areal average of SVF and temperature differences has a closer correlation than point comparison. Lindberg (2007) alternatively considered the circular average of SVF and adapted the radii of 50 and 100 m for a 1.4×1.4 km site. Because of the similar size of the studied site, we have taken Lindberg's approach. Four radii are tested to compare the applicability of the areal average of SVF in different scales, being 50, 100, 150 and 200 m. The generated continuous SVF map allows us to carry out spatial analysis of this kind and the GIS-based data makes the operation easy and straightforward with the help of the ArcGIS system. The respective regression results are shown in Table IV.

The renewed regression analysis with a 50-m radius average shows a significant increase in correlation, with determination coefficient in the order of 0.49, which also confirms Unger's findings from another aspect. The correlation is further improved by a 100-m radius average ($R^2 \sim 0.65$) and a 150-m radius average ($R^2 \sim 0.66$), whereas a 200-m radius average gives a substantial decline ($R^2 \sim 0.53$). Considering the scale of the study and the computing time, the 100 m radius is chosen in practice. Figure 8 shows the neighbourhood average SVF map with a 100 m radius. The regression function is given by Equation (10).

$$\Delta T = -6.6595 \times \mathrm{SVF}_{100\mathrm{m\_neigh\_avg}} + 5.6061,$$
$$R^2 = 0.65 \ (0.2 \ \leq \ \mathrm{SVF} \ \leq \ 0.75) \qquad (10)$$

The regression coefficient of -6.6595 indicates that SVF is inversely proportional to daytime air temperature differences: an $\sim$0.15 decrease of a 100-m radius neighbourhood average of SVF may result in a 1 °C temperature elevation.

4.3. Verification and calibration

Another field measurement was carried out in TST in 2008. The same equipments were used as in the previous measurement but this time mounted on a mobile meteorological station fixed at 2 m above ground level (Figure 9). Ten-minute average data were recorded. Similar measurement routes were taken but a smaller set of 12 points were monitored. For data analysis, two points close to a high traffic road and two points close to the exits of a major metro station are deleted. Eight points are used in the regression analysis. On the basis of the findings in Section 4.2, the 100-m radius average SVF is adapted and a regression equation is derived with 5% significance level, as given by Equation (11).

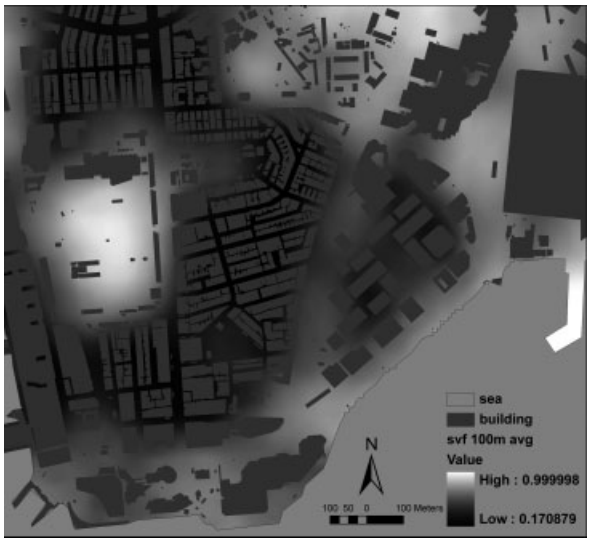

Figure 8. 100-m radius neighbourhood average SVF map for TST site.

$$\Delta T = -5.2793 \times \mathrm{SVF}_{100\mathrm{m\_neigh\_avg}} + 4.644,$$
$$R^2 = 0.82 \ (0.25 \ \leq \ \mathrm{SVF} \ \leq \ 0.76) \qquad (11)$$

The relationship generally agrees with Equation (10). However, the relatively small sample size may not reflect the details of the relationship. In this sense it is merged with the 2006 dataset, and a calibrated regression with a 5% significance level is derived based on the total 49 points. The regression equation is given by Equation (12)

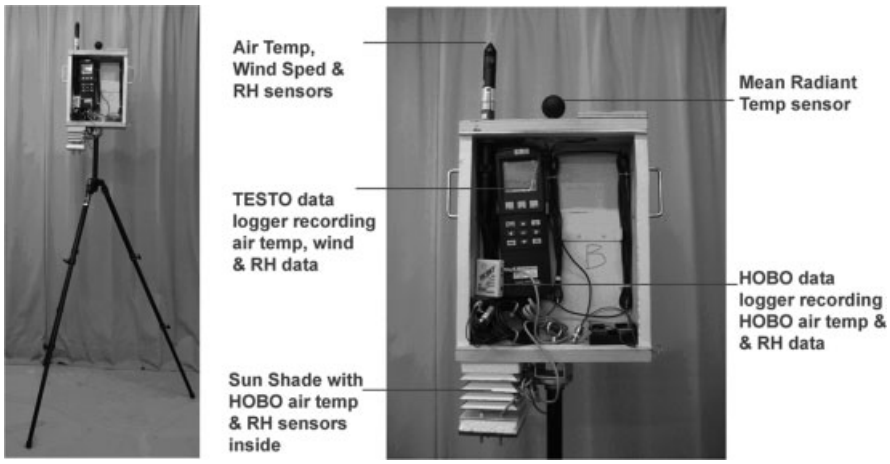

Figure 9. Mobile meteorological station used in the field measurement. Equipments used in this study are the TESTO sensor and the TESTO data logger.

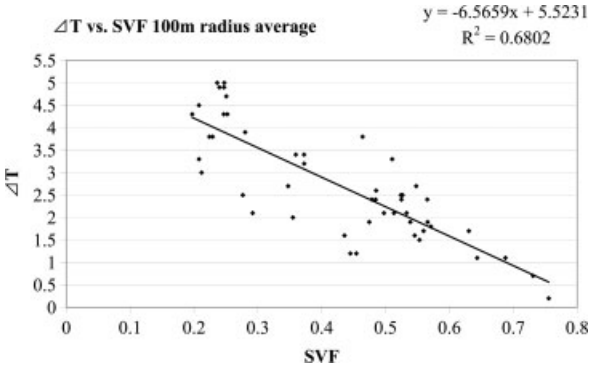

Figure 10. Correlation of ΔT and 100-m radius neighbourhood average SVF value.

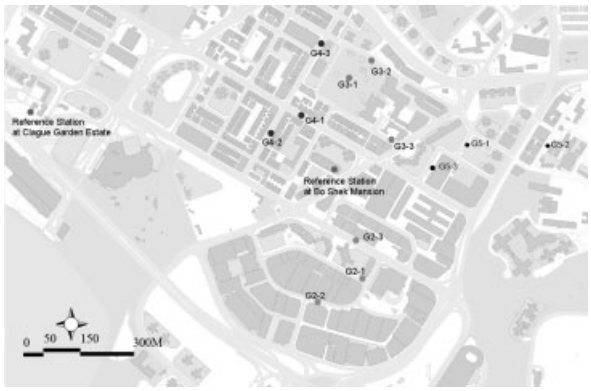

Figure 11. Temperature measurement map for TW site.

(with 5% significance level), and an illustration of the correlation is shown in Figure 10.

$$\Delta T = -6.5659 \times \mathrm{SVF}_{100\mathrm{m\_neigh\_avg}} + 5.5231,$$
$$R^2 = 0.68 \ (0.2 \ \leq \ \mathrm{SVF} \ \leq \ 0.76) \qquad (12)$$

4.4. Validation analysis in TW

Two field measurements were carried out in the TW site on the calm summer afternoons on 15 May 2008 and 21 June 2008 to further understand the derived relationship between SVF and intra-urban temperature differences. Climatic conditions of the measurements are given in Table V.

A total number of 12 points in built-up areas were measured for both the cases (Figure 11). The mobile meteorological station was used. The lowest air temperature was observed at the reference point which was located at a relatively open space. Temperature differences for the 12 measured points are calculated. By checking the map, it is found that point G4-2 (as shown in Figure 10, similarly hereinafter) is next to a mini-bus stop, point G4-3 is next to a bus stop and a mall exit, point G5-1 and G5-3 are next to car parking lots and point G5-2 is next to a bus stop. These five points involve other factors than the thermal load of buildings. Another look at the temperature differences also confirms the extreme high temperature differences (ranging from 3.3 °C to 6.1 °C for 15 May 2008 and 4.1 °C to 6.6 °C for 21 June 2008). So these points are not used in the validation analysis. For the analysed seven points, 2-day average temperatures are used.

A 100-m radius neighbourhood average SVF for each point is calculated. It is found that point G2-2 has an SVF of 0.1109, which is outside the valid SVF range of Equation (12), so this point is excluded from the analysis. Estimated ΔTs are calculated based on Equation (12) and the results are compared with the measured ΔTs. The comparison is given in Table VI. The comparison shows that except for only one point (G3-3), the estimated ΔTs agree with the measured ΔTs reasonably well. Despite the large discrepancy found at point G3-3, other points with similar SVFs (G2-1 and G4-1) show better agreements. It is currently not clear what causes the discrepancy for the single point; nevertheless, it is confirmed that the derived relationship has reasonable explanatory power in revealing the impact of SVF on daytime intra-urban air temperature differences. In the following discussions, Equation (12) is used as the ΔT–SVF relationship for Hong Kong.

Table VI. Comparison between measured and estimated temperature differences in TW.

Point ID	SVF	Measured ΔT (°C)	Estimated ΔT (°C)	Error (°C)
G2-1	0.266893	4.1	3.8	−0.3
G2-3	0.237072	4.0	4.0	0
G3-1	0.5695027	1.5	1.8	0.3
G3-2	0.524757	1.9	2.1	0.2
G3-3	0.295635	2.6	3.6	1
G4-1	0.272	4.2	3.7	−0.5

The SVF values are 100-m radius neighbourhood averages. Point IDs are as shown in Figure 11. Measured ΔTs are the average of two-day measurements, and estimated ΔTs are calculated based on Equation (12).

Table V. Summary of climatic conditions of field measurement in TW, including air temperature (T), global solar radiation (Radiation), relative humidity (RH), wind speed (V) and duration of sunshine (Sunshine).

Date	Measurement period	T (°C)	Radiation (W/m^2)	RH (%)	V (m/s)	Sunshine (h)
15 May 2008	14 : 30–15 : 30	≈28.7	500–750	≈60	0–2	11.2
21 June 2008	14 : 30–15 : 30	30–31.7	670–900	65–70	2.7–3.3	10.9

The data were recorded by the Hong Kong Observatory at a station next to the study area.

4.5. Discussions on the revealed relationship

What is noticeable is that the analysis reveals a strong 'negative' relationship between SVF and daytime intra-urban air temperature differences, as opposed to the 'positive' relationships found in early studies in Hong Kong (Giridharan *et al*., 2004, 2007). Despite the fact that Giridharan *et al*.'s statements on the impact of SVF will be made more pertinent if the diversity of the other influential factors could be controlled properly, our findings also contradict the intuition that a more open surface receives more solar insolation during daytime and therefore will heat up the local air and lead to higher temperatures than a more obstructed surface. The exact cause for the observed 'negative' relationship is not clear at the moment. However, we speculate that it will be attributed to two aspects. Firstly, previous studies have shown through parametric models that the surface albedo of an urban setting is lower than that of a flat setting (Ashie and Itoh, 2009), and the urban albedo of an urban geometry with a 50% building-to-land ratio is significantly lower than that with a 12.5% ratio (Itoh and Ashie, 2009). In this sense, Hong Kong's extremely high-rise and high-density urban geometry is expected to contribute to heat trapping and therefore high temperature elevation in built-up areas. Secondly, Hong Kong is a windy coastal city with wind speeds >3 m/s commonly observed in open spaces. The building bulks significantly alter the wind environment and may impact air advection and therefore heat transfer. This may also be one reason for the temperature differences between different urban settings. While SVF is used as an indicator to quantify urban geometry's impact on air temperature variations, there is more work to be done to refine this understanding and also to characterize this phenomenon in an energy balance frame, for instance, to study the impact of other influential factors, such as building surface albedo, advection, local anthropogenic heat, etc.

5. Application discussion

This section addresses discussions with concerns on the application of the present SVF analysis on urban design and planning. Firstly, on the zonal scale, it derives an overall intra-urban air temperature difference pattern of Hong Kong by categorizing Hong Kong's whole urban area into classes quantified by SVF. Secondly, on the building scale, it carries out a parametric study to achieve larger SVF in street canyons without reducing building volume and gives configuration recommendations in planning practice.

5.1. Zonal-scale application

On the basis of the findings in the case study, an overall intra-urban air temperature difference pattern of Hong Kong could be derived when employing neighbourhood average of SVF as a quantifier. In this sense, we selected Hong Kong's most concerned areas, including the downtown area, residential development and new town, and simulated SVF for these sites. The result is then classified based on Equation (12), where SVF <0.35 indicates 3 °C temperature elevation, SVF within (0.35, 0.50) indicates 2 °C temperature elevation, SVF within (0.50, 0.65) indicates 1 °C temperature elevation, and SVF >0.65 indicates no temperature elevation within the urban area. Areas with SVF value outside the valid SVF range ($0.2 \leq \text{SVF} \leq 0.76$) are not considered. This classification gives a conservative estimation of temperature variation due to urban geometry. The temperature variation pattern map is shown in Figure 12. This map could provide quantitative information in zonal planning with concerns on thermally sensitive areas.

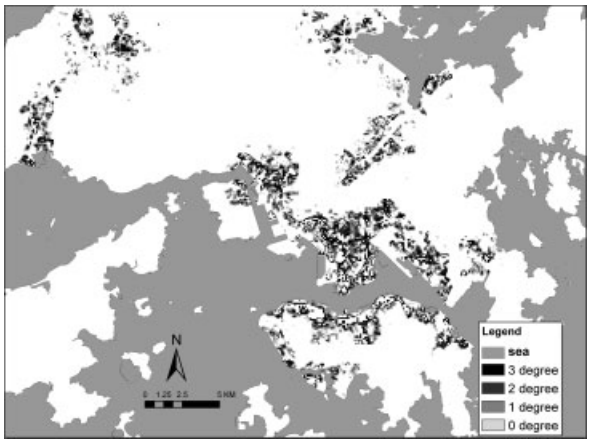

Figure 12. Intra-urban temperature variation pattern of Hong Kong's most concerned areas.

For planners, the spatial intra-urban temperature map can be particularly revealing. Firstly, it shows how building volume and therefore the resulting SVF can affect temperature variation, and thus human thermal comfort, or thermal stress. A 3 °C intra-urban temperature rise is significant. In hot and humid Hong Kong, this can lead to elevated heat stress-related mortality and morbidity (Leung *et al*., 2008). It can also exaggerate the occurrence of day heat spells (defined as seven continuous occurrences of very hot days [$T_{max} \geq 33$ °C]) and night heat spells (defined as seven continuous occurrences of very hot nights [$T_{min} \geq 28$ °C]). Ng (2009) has noted that the number of heat spells in terms of very hot days and very hot nights has an exponential relationship with the intra-urban temperature elevation of the locality above the ambient. That is to say, the impact of any intra-urban temperature rise due to the UHI effect can be serious in Hong Kong.

Secondly, the understanding of the intra-urban temperature differentials spatially can allow planners and politicians a better appreciation of action strategically. Focus areas can be better identified and detailed investigations and mitigation measures can be better implemented. For instance, in the current review exercise of the Outline Zoning Plans of Hong Kong, the understanding allows Hong Kong planners to better state the needs of urban

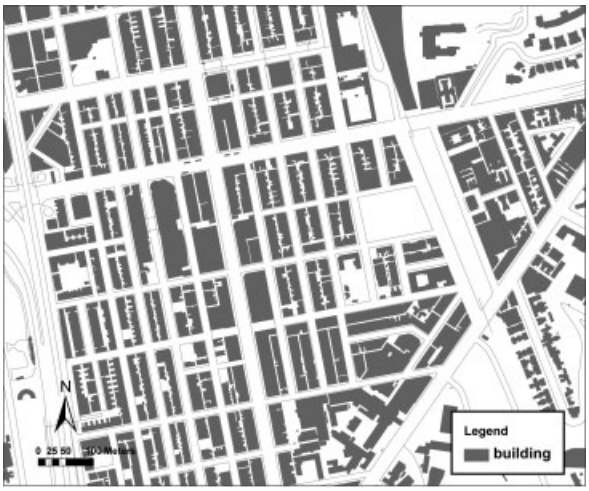

Figure 13. Plan of Mong Kok, Hong Kong.

greeneries, urban 'oasis', building setback and urban air paths where they are most needed.

Thirdly, based on the thermal load understanding, planners of Hong Kong are now incorporating it into the Hong Kong Urban Climatic Map that synergizes the thermal understanding with the dynamic understanding to create the bio-meteorological map of urban Hong Kong (Ng *et al*., 2008a). Better quantifications of cost–benefit and value-based actions could then be developed.

5.2. Building-scale application

Furthermore, a parametric study is carried out to test the SVF of different building configurations. The development site in the study is selected to be 50×100 m and the street width is 16 m. These settings are representative of some congested urban areas, for example Mong Kok, in Hong Kong (Figure 13).

A total number of 14 types of building configurations (a tower with a podium) are tested. Parameter settings are given in Table VII. The selections of parameters are based on Hong Kong's building regulations (Department of Justice, The Government of Hong Kong S.A.R., 2005). The buildings are all homogenous blocks symmetrically laid out on an infinite plane (Figure 14).

The building volume of a site is estimated to be 300 000 m^3, with a plot ratio of 15 and a floor-to-floor height of 4 m. This volume value is used as unity in our study. The building is raised with a height corresponding to a 10% building volume increment from 10 to 200% for all the 14 configurations. Maximum podium height is selected to be 15 m. All parametric settings follow typical and representative professional practice in Hong Kong following the building regulations.

The quantity here of interest is the 100-m radius neighbourhood average of SVF value at the centre point of a 2×2 site matrix, representing the case of a street canyon (Figure 14). In order to obtain a correct 100-m radius neighbourhood average, a 10×6 matrix is simulated in practice to eliminate marginal error. Comparisons of simulated SVF for 14 configurations are shown in Figure 15. A zoom-in of the section with building volume from 40 to 110% is shown in Figure 16. Comparisons of total building height are shown in Figure 17.

It is shown in Figure 15 that, in general, SVF and building volume follow a logarithmic relationship: when building volume is below 80%, SVF decreases rapidly as building volume increases; after building volume is over 80%, the change in SVF with the increase in building volume is relatively small. The building volume range is divided into four categories representing different plot ratio spectrum: building volume smaller than 33% representing plot ratio smaller than 5, building volume from 33 to 60% representing plot ratio from 5 to 9, building volume from 60 to 80% representing plot ratio from 9 to 12 and building volume larger than 80% representing plot ratio >12. For the four categories, the change in SVF in terms of building volume could be quite different; this indicates that the understanding of SVF as a determining factor for thermal load should be different for low and high-density urban environments.

Another finding is that building configurations with a great-coverage podium and a great-coverage tower will result in lowest SVF, as shown in the cases of P1T1, P1T2 and P2T2; on the other hand the differences of SVF for other building configurations are very small. Figure 16 shows a section with building volume from

Table VII. Characteristics of 14 building configurations.

P \ T	Size 1	Size 2	Size 3	Size 4	Size 5
Size 1	Configuration (P1T1)	Configuration (P1T2)	Configuration (P1T3)	Configuration (P1T4)	Configuration (P1T5)
Size 2	–	Configuration (P2T2)	Configuration (P2T3)	Configuration (P2T4)	Configuration (P2T5)
Size 3	–	–	Configuration (P3T3)	Configuration (P3T4)	Configuration (P3T5)
Size 4	–	–	–	Configuration (P4T4)	Configuration (P4T5)

P, podium; T, tower.
Size 1 = 50×100 (m^2) = 100% site coverage.
Size 2 = 46×96 (m^2) = 88.3% site coverage.
Size 3 = 40×90 (m^2) = 72% site coverage.
Size 4 = 34×84 (m^2) = 57.1% site coverage.
Size 5 = 24×74 (m^2) = 35.5% site coverage.

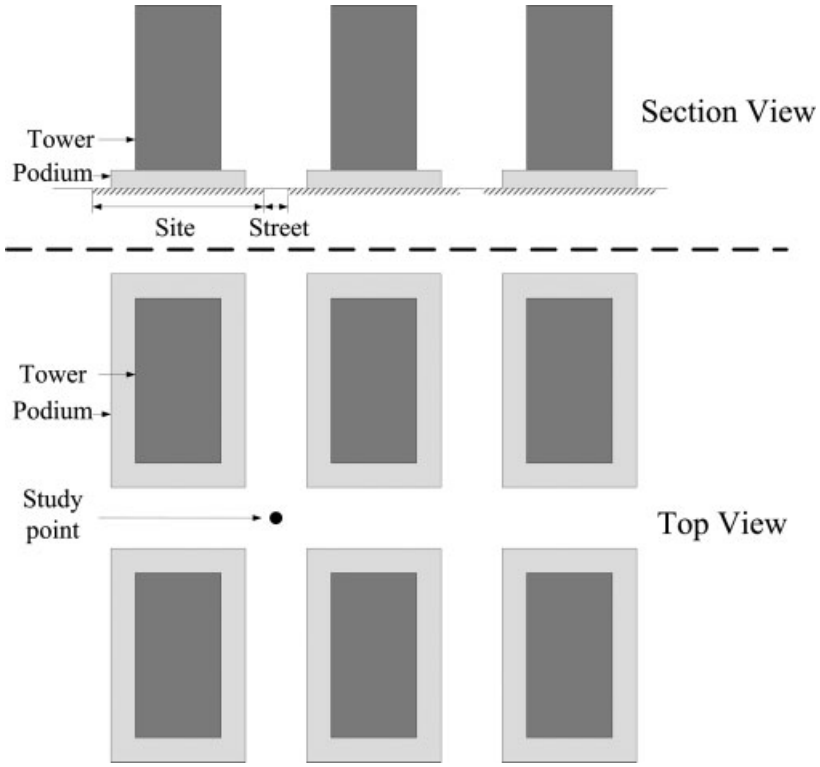

Figure 14. Section view and top view of building blocks in the parametric study. Site size is 100 × 50 m, street width is 16 m and a building block consists of a tower and a podium. Figures are not drawn to scale.

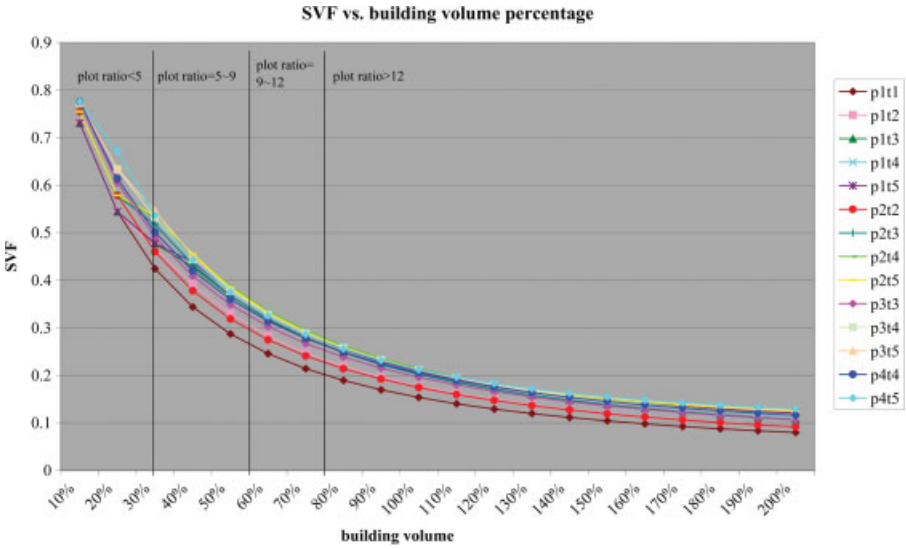

Figure 15. Comparison of 100-m radius neighbourhood average SVF at the study point for 14 configurations. The building volume is classified into four categories representing four plot ratio ranges. This figure is available in colour online at wileyonlinelibrary.com/journal/joc

40 to 110%, which is representative for typical cases in Hong Kong. It reveals that the reduction of site coverage will have a significant benefit in achieving larger SVF and the maximum SVF difference of different building configurations could be up to 0.1, which will cause an ∼0.6 °C temperature difference based on our study (refer to Equation (12)).

Figure 17 shows a comparison of the total building height of 14 configurations. It could be generally stated that small site coverage tower will increase the total building height significantly if building volume is not to be reduced. Recommendations of building configurations are given in Table VIII by considering both SVF and building height. An illustration of the recommendation is shown in Figure 18.

6. Conclusion

In this study, a simulation approach is taken to investigate the impact of SVF on summer daytime intra-urban air

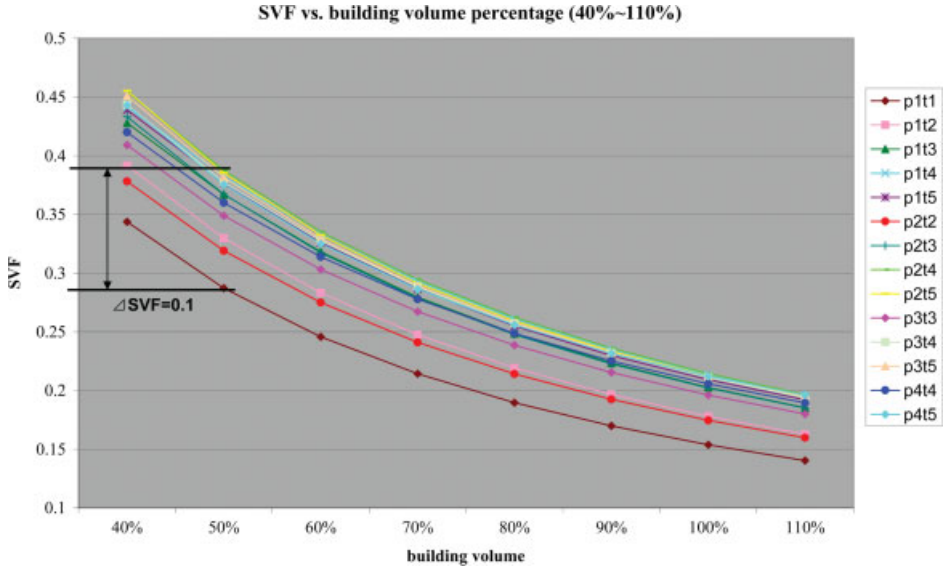

Figure 16. Comparison of 100-m radius neighbourhood average SVF at study point for 14 configurations (building volume: 40–110%). This figure is available in colour online at wileyonlinelibrary.com/journal/joc

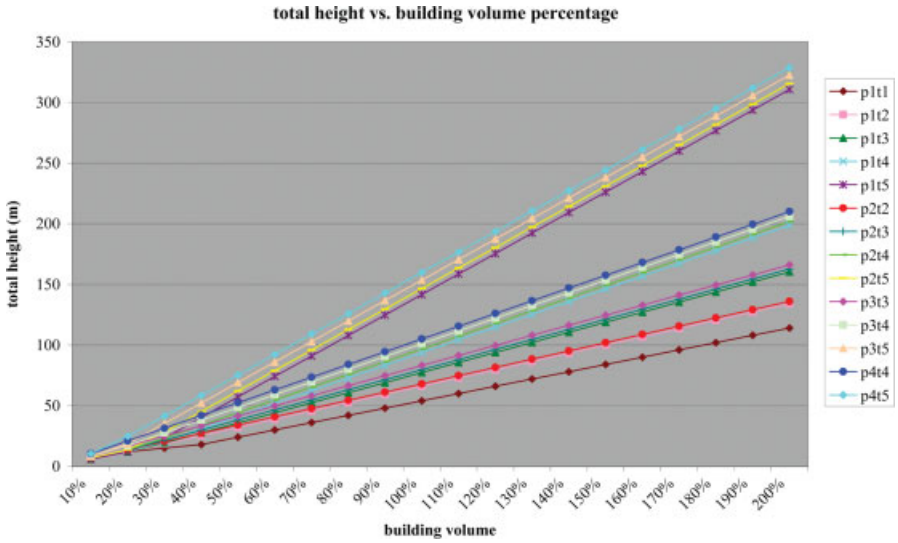

Figure 17. Comparison of total building height for 14 configurations. This figure is available in colour online at wileyonlinelibrary.com/journal/joc

temperature variations in high-rise and high-density areas in Hong Kong. The analysis reveals that SVF is inversely proportional to the daytime intra-urban temperature differences, and the areal average of SVF has a stronger explanatory power in quantifying this relationship than point SVF, i.e. a decrease of ∼0.15 in a 100-m radius neighbourhood average of SVF may result in 1 °C temperature elevation. The study suggests that areal average of SVF could be used as a determining factor to predict temperature variations to a substantial degree. Planning applications of zonal and building scales are also presented.

A limitation of this study is that it only focuses on densely built-up areas where little vegetation exists. When vegetation data is present, further work should be carried out such as correcting the SVF calculating method accordingly and analysing the effect of vegetation on temperature variations. The findings are also expected to be refined by conducting a longer term of observation to enlarge dataset and examining the impact of other influential factors.

To sum up, the study shows that SVF analysis is a useful and effective tool for urban climatology studies in high-rise and high-density sub-tropical cities, and the extensive spatial analysis is only possible with the software method in a GIS framework. It is also shown that SVF analysis can provide support for the development of planning standards. With this intention, the method is implemented as an ArcGIS-embedded tool, which is familiar to planners and does not require extra knowledge of computation or programming skills.

As a final remark, the software method has been proved to be suitable for analysing the spatial variability of urban forms. In a more general sense, the simulation approach

Table VIII. Characteristics and recommendations of building configurations.

Group	Characteristics	Effect	Recommended
1: P1T1, P1T2, P2T2	Large podium with large tower	Small SVF	No: high thermal load
2: P2T3, P2T4, P3T3, P3T4, P4T4	Medial podium with medial tower	Large SVF with reasonable height	Yes: low thermal load and aesthetic form
3: P1T5, P2T5, P3T5, P4T5	Small tower	Excessive height	No: unaesthetic form

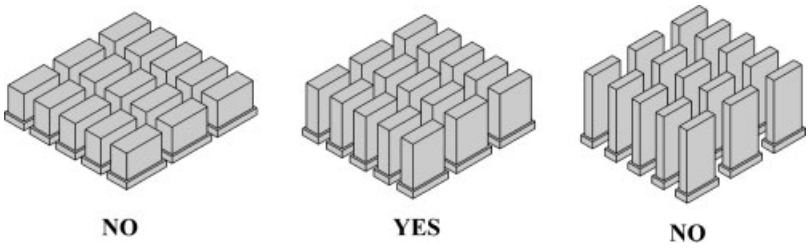

Figure 18. An illustration of building configuration recommendation.

opens up new possibilities for characterizing quantities and relationships in urban studies. GIS-based tools, used in collaborattion with other whole building simulation and modelling methods such as computational fluid dynamics, are expected to provide a more comprehensive understanding of urban systems.

Acknowledgements

The study is supported by a PGS grant from The Chinese University of Hong Kong and a contract research grant from the Planning Department of the Government of Hong Kong S. A. R. The authors wish to thank the Planning Department of Hong Kong for providing the building data and the Hong Kong Observatory for the weather data needed for the study. In particular, the authors wish to thank Mr Marcin Rzepa for providing the access to the BMSky-view software, and Mr Vincent Cheung for providing the fish-eye photos. The authors also wish to give special thanks to the two referees for their valuable comments which help to improve the paper a lot.

References

Alonso MS, Labajo JL, Fidalgo MR. 2003. Characteristics of the urban heat island in the city of Salamanca, Spain. *Atmosfera* **16**: 137–148.

Anderson MC. 1964. Studies of the woodland light climate: I. The photographic computation of light conditions. *Journal of Ecology* **52**: 27–41.

Ashie Y, Itoh D. 2009. Study on the characteristics of solar radiation in the geometrically complex urban spaces by using a spectroradiometer. *Paper presented at 2nd International Conference on Countermeasures to Urban Heat Islands. Lawrence Berkeley National Laboratory*, Berkeley, California, 21–23 September 2009.

Atkinson BW. 2003. Numerical modelling of urban heat-island intensity. *Boundary-Layer Meteorology* **109**: 285–310.

Bärring L, Mattsson JO, Lindqvist S. 1985. Canyon geometry, street temperatures and urban heat island in Malmö, Sweden. *Journal of Climatology* **5**: 433–444.

Blennow K. 1995. Sky view factors from high-resolution scanned fish-eye lens photographic negatives. *Journal of Atmospheric and Oceanic Technology* **12**: 1357–1362.

Bourbia F, Boucheriba F. 2010. Impact of street design on urban microclimate for semi arid climate (Constantine). *Renewable Energy* **35**: 343–347.

Census and Statistics Department, The Government of Hong Kong S.A.R. 2009. *Hong Kong in Figures: Population and Vital Events*, Retrieved March 4, 2010. Available at http://www.censtatd.gov.hk/FileManager/EN/Content_803/population.pdf.

Chan JCL, Ng T. 1991. Temperature variability over Hong Kong. *Hong Kong Meteorological Society Bulletin* **1**: 14–25.

Chapman L, Thornes JE. 2004. Real-time sky-view factor calculation and approximation. *Journal of Atmospheric and Oceanic Technology* **21**: 730–742.

Chapman L, Thornes JE, Bradley AV. 2001. Rapid determination of canyon geometry parameters for use in surface radiation budgets. *Theoretical and Applied Climatology* **69**: 81–89.

Chapman L, Thornes JE, Bradley AV. 2002. Sky-view factor approximation using GPS receivers. *International Journal of Climatology* **22**: 615–621.

Chow WTL, Roth M. 2006. Temporal dynamics of the urban heat island of Singapore. *International Journal of Climatology* **26**: 2243–2260.

Department of Justice, The Government of Hong Kong S.A.R. 2005. *Building Regulations: Regulations 18A, 20 & 21. Percentage Site Coverage and Plot Ratios*, Retrieved March 2010. Available at http://www.legislation.gov.hk/blis_ind.nsf/e1bf50c09a33d3dc48256-4840019d2f4/f781dda725aeff70482570f3000e4d27?OpenDocument.

Eliasson I. 1990–1991. Urban geometry, surface temperature and air temperature. *Energy and Buildings* **15**: 141–145.

Eliasson I. 1996. Urban nocturnal temperatures, street geometry and land use. *Atmospheric Environment* **30**: 379–392.

Fung WY, Lam KS, Nichol J, Wong MS. 2009. Derivation of nighttime urban air temperatures using a satellite thermal image. *Journal of Applied Meteorology and Climatology* **48**: 863–872.

Gal T, Lindberg F, Unger J. 2009. Computing continuous sky view factors using 3D urban raster and vector databases: comparison and application to urban climate. *Theoretical and Applied Climatology* **95**: 111–123.

Gal T, Rzepa M, Gromek B, Unger J. 2007. Comparison between sky view factor values computed by two different methods in an urban environment. *ACTA Climatologica Et Chorologica* **40**(41): 17–26.

Giridharan R, Ganesan S, Lau SSY. 2004. Daytime urban heat island effect in high-rise high-density developments in Hong Kong. *Energy and Buildings* **36**: 525–534.

Giridharan R, Lau SSY, Ganesan S, Givoni B. 2007. Urban design factors influencing heat island intensity in high-rise high-density environments of Hong Kong. *Building and Environment* **42**: 3669–3684.

Government of Hong Kong S. A. R. 2009. *Hong Kong: The Facts – Population*, Retrieved March 2010. Available at http://www.gov.hk/en/about/abouthk/factsheets/docs/population.pdf.

Grimmond CSB, Potter SK, Zutter HN, Souch C. 2001. Rapid methods to estimate sky-view factors applied to urban areas. *International Journal of Climatology* **21**: 903–913.

Hart MA, Sailor DJ. 2009. Quantifying the influence of land-use and surface characteristics on spatial variability in the urban heat island. *Theoretical and Applied Climatology* **95**: 397–406.

Hong Kong Observatory. 2010. *Monthly Normals of Meteorological Elements 1971–2000*, Retrieved March 2010. Available at http://www.weather.gov.hk/cis/normal/1971_2000/enormal08.htm.

Itoh D, Ashie Y. 2009. Study on the spectral albedo in the geometrically complex urban spaces. *Paper presented at the 7th International Conference on Urban Climate*. Yokohama, Japan, 29 June–3 July 2009.

Johnson GT, Watson ID. 1984. The determination of view factors in urban canyons. *Journal of Climate and Applied Meteorology* **2**: 329–335.

Leung W-M, Lee T-C. 2010. Urbanization and City Climate: A Diurnal and Seasonal Perspective.In *Designing High-Density Cities : For Social and Environmental Sustainability*, Ng E (ed). Earthscan: London; Sterling, VA.

Leung YK, Yip KM, Yeung KH. 2008. Relationship between thermal index and mortality in Hong Kong. *Meteorological Applications* **15**: 399–409.

Lindberg F. 2005. Towards the use of local governmental 3-D data within urban climatology studies. *Mapping Image Science* **2**: 32–37.

Lindberg F. 2007. Modelling the urban climate using a local governmental geo-database. *Meteorological Applications* **14**: 263–273.

Lindqvist S. 1970. *Bebyggelseklimatiska Studier (English Summary: Climatological Studies of Built-up Areas*): Meddelanden från Lunds universitets geografiska institution. Avhandlingar, LXI. CWK Gleerup. Lund.

Mayor of London. 2006. London's Urban Heat Island : A Summary for Decision Makers. Greater London Authority: London.

Morris CJG, Simmonds I. 2000. Associations between varying magnitudes of the urban heat island and the synoptic climatology in Melbourne, Australia. *International Journal of Climatology* **20**: 1931–1954.

Murphy DJ, Hall MH, Hall CAS, Heisler GM, Stehman SV, Anselmi-Molina C. 2010. The relationship between land cover and the urban heat island in northeastern Puerto Rico. *International Journal of Climatology* DOI:10.1002/joc.2145 (in press).

Ng E. 2009. Wind and heat environment in densely built urban areas in Hong Kong (invited paper). *Global Environmental Research. A Special Issue on Wind Disaster Risk and Global Environment Change* **13**: 169–178.

Ng E, Kwok K, Sun D, Yau R, Katzschner L. 2008a. Draft urban climatic analysis map. Urban climatic map and standards for wind environment – feasibility study, Working Paper No. 1A, Technical Report for Planning Department HKSAR.

Ng E, Wang U, Ren C, Cheng V. 2008b. Technical input report : methodologies and results of field measurement. Urban climatic map and standards for wind environment – feasibility study. Technical Report for Planning Department HKSAR.

Oke TR. 1981. Canyon geometry and the nocturnal heat island: comparison of scale model and field observations. *Journal of Climatology* **1**: 237–254.

Oke TR. 1987. *Boundary Layer Climates*, 2nd edn, Methuen: London.

Planning Department, The Government of Hong Kong S.A.R. 2008. *Broad Land Usage Distribution*. Available at http://www.pland.gov.hk/pland_en/info_serv/statistic/landu.html [accessed May 1999].

Ratti C, Richens P. 1999. Urban texture analysis with image processing techniques. *Paper presented at CAAD Futures 99*. Atlanta, GA.

Rzepa M. 2009. The map of sky view factor in the center of Lodz. *Paper presented at the 7th International Conference on Urban Climate*. Yokohama, Japan, 29 June–3 July 2009.

Santos IG, Lima HG, Assis ES. 2003. A comprehensive approach of the sky view factor and building mass in an urban area of the city of Belo Horizonte, Brazil. In *Proceedings of the 5th International Conference on Urban Climate*. University of Lodz, Lodz, 367–370.

Stathopoulou M, Cartalis C. 2007. Daytime urban heat islands from Landsat ETM+ and Corine land cover data: an application to major cities in Greece. *Solar Energy* **81**: 358–368.

Steemers K, Ramos M, Sinou M. 2004. Urban diversity. In *Environmental Diversity in Architecture*, Steemers K, Steane MA (eds). Spon Press: London; New York.

Steyn DG. 1980. The calculation of view factors from fish-eye lens photographs. *Atmosphere-Ocean* **18**: 254–258.

Steyn DG, Hay JE, Watson ID, Johnson GT. 1986. The determination of sky view-factors in urban environments using video imagery. *Journal of Atmospheric and Oceanic Technology* **3**: 759–764.

Streutker DR. 2003. Satellite-measured growth of the urban heat island of Houston, Texas. *Remote Sensing Environment* **85**: 282–289.

Svensson MK. 2004. Sky view factor analysis – implications for urban air temperature differences. *Meteorological Applications* **11**: 201–211.

Unger J. 2004. Intra-urban relationship between surface geometry and urban heat island: review and new approach. *Climate Research* **27**: 253–264.

Unger J. 2009. Connection between urban heat island and sky view factor approximated by a software tool on a 3D urban database. *International Journal of Environment and Pollution* **36**: 59–80.

Upmanis H, Chen D. 1999. Influence of geographical factors and meteorological variables on nocturnal urban-park temperature differences – a case study of summer 1995 in Göteborg, Sweden. *Climate Research* **13**: 125–139.

Vieira H, Vasconcelos J. 2003. Urban morphology characterisation to include in a GIS for climatic purposes in Lisbon. Discussion of two different methods. In *Proceedings of the 5th International Conference on Urban Climate*. University of Lodz, Lodz, 417–420.

Watson ID, Johnson GT. 1987. Graphical estimation of sky view-factors in urban environments. *International Journal of Climatology* **7**: 193–197.

Wu MC, Leung YK, Lui WM, Lee TC. 2008. A study on the difference between urban and rural climate in Hong Kong. *Paper presented at the 22th Yue-Kong Meteorological Technology Meeting*. Zhongshan, China, 22–23 January 2008.

Yamashita S, Sekine K, Shoda M, Yamashita K, Hara Y. 1986. On the relationships between heat island and sky view factor in the cities of Tama River Basin, Japan. *Atmospheric Environment* **20**: 681–686.

Yang F, Lau SSY, Qian F. 2010. Summertime heat island intensities in three high-rise housing quarters in inner-city Shanghai China: building layout, density and greenery. *Building and Environment* **45**: 115–134.

